Reactivity Studies of $[Co@Sn_9]^{4-}$ with Transition Metal Reagents: Bottom-Up Synthesis of Ternary Functionalized Zintl Clusters

Chao Liu,[a,b,†] Lei-Jiao Li,[a,†] Xiao Jin,[c] John E. McGrady,[*c] and Zhong-Ming Sun [*a,d]

[a] State Key Laboratory of Rare Earth Resource Utilization, Changchun Institute of Applied Chemistry, Chinese Academy of Sciences, 5625 Renmin Street, Changchun, Jilin 130022, China.

[b] University of Chinese Academy of Sciences, Beijing 100049, P. R. China.

[c] Department of Chemistry, University of Oxford, South Parks Road, Oxford, OX1 3QZ, United Kingdom.

[d] State Key Laboratory of Coordination Chemistry, School of Chemistry and Chemical Engineering, Nanjing University, Nanjing 210023, P. R. China.

ABSTRACT: The binary cluster $[Co@Sn_9]^{4-}$ (**1**) was extracted directly from ethylenediamine (en) solutions of an intermetallic precursor with nominal composition "$K_5Co_3Sn_9$", and its reactions with various organometallic reagents were explored. Reaction with $Ni(PPh_3)_2(CO)_2$ gives $[Co@Sn_9Ni(CO)]^{3-}$ (**2**), a Co-centered *closo*-Sn_9Ni bicapped square antiprism. Analogous reactions with $Ni(COD)_2$, $Pt(PPh_3)_4$ and $Au(PPh_3)Ph$ led to the isolation of $[Co@Sn_9Ni(C_2H_4)]^{3-}$ (**3**), $[Co@Sn_9Pt(PPh_3)]^{3-}$ (**4**) and $[Co@Sn_9AuPh]^{3-}$ (**5**), respectively. **3** is structurally similar to **2** but significantly distorted from a *closo*-cluster with one open square face. The coordination of $[CoSn_9]^{3-}$ by $PtPPh_3$ (**4**) or AuPh (**5**) induces a structural transformation in the $CoSn_9$ core, from a monocapped square antiprism (C_{4v}) to a tricapped trigonal prismatic structure (*pseudo*-C_{3v}), with the transition metal fragment capping a triangular face. The four trimetallic anions presented here represent a new family of ternary functionalized Zintl clusters incorporating a d^9 transition metal centre. All clusters were characterized by single-crystal X-ray diffraction and electrospray ionization mass spectrometry (ESI-MS).

Introduction

The solution-phase chemistry of polyanion clusters of the group 14/15 elements has advanced enormously in the last decade, the interest being driven primarily by their structural diversity and unusual electronic properties.[1-3] Amongst these clusters, the nine-atom family $[E_9]^{n-}$ (E= Si-Pb, n= 2, 3 or 4) is of particular interest because they are easily accessible in a range of charge states (n), and their geometries are very flexible.[4] The earlies studies of the reactivity of $[E_9]^{n-}$ clusters with d^6 transition metal reagents such as $LM(CO)_3$ (M= Cr, Mo, W; L= mesitylene, cycloheptatriene or toluene) resulted in functionalized cluster anions, $[E_9M(CO)_3]^{4-}$ (E = Sn, Pb; M = Cr, Mo, W), [5] where the $M(CO)_3$ fragments occupy vertex sites (either capping or equatorial) of ten atom clusters. Subsequent work with late- and post-transition metal species also yielded a series of related metal fragment functionalized clusters including $[\{Ni(CO)_2\}_2(u\text{-}Si_9)_2]^{8-}$,[6] $[Ge_9Ni(CO)]^{3-}$,[7] $[Ge_9Pd(PPh_3)]^{3-}$,[8] $[Sn_9Ir(COD)]^{3-}$,[9a] $[Ge_9Cu(PR_3)]^{3-}$ (R = ^{i}Pr, Cy)[9b] and $[E_9ZnR]^{3-}$ (R = Mes, ^{i}Pr, Ph).[10] Attempts to center these $[E_9]^{x-}$ clusters using transition metals have also led to a series of ligand-free intermetalloid cluster with fascinating polyhedral structures,[11] including the unique 12-vertex fullerene-like clusters[12] $[M@Pb_{12}]^{2-}$ (M = Ni, Pt, Pd),[13] which were synthesized by reaction of $[Pb_9]^{4-}$ with ML_4 (M = Ni, Pd, Pt; L= PPh_3). Other examples of ligand-free group 14 Zintl ions centered by transition metal atoms include $[Ni@E_9]^{x-}$ (E = Ge, Sn),[14] $[Cu@E_9]^{3-}$ (E = Sn, Pb),[15] $[Ni@Pb_{10}]^{2-}$,[16] $[Ir@Sn_{12}]^{3-}$,[8] $[Mn@Pb_{12}]^{3-}$,[17] *β*–$[Co_2@Ge_{16}]^{4-}$,[18] $[M_2@Sn_{17}]^{x-}$ (M = Ni, Pt, Co),[19] $[Pd_2@E_{18}]^{4-}$ (E = Ge, Sn)[20] and $[Ni_3@Ge_{18}]^{4-}$,[14a] as well as the 3-connected non-deltahedral clusters $[Co@Ge_{10}]^{3-}$,[21] $[Fe@Ge_{10}]^{3-}$,[22] $[Ru@Ge_{12}]^{3-}$.[23] and *a*–$[Co_2@Ge_{16}]^{4-}$.[18]

The empty nine-atom group 14 Zintl ions，particularly the germanium species $[Ge_9]^{n-}$, also can be functionalized by formation of a 2-center-2-electron exo-bond using main-group organometallic fragments[24] or even organic species.[25- 27] $[Ph_2Bi\text{-}(Ge_9)\text{-}BiPh_2]^{2-}$ was the first main-group functionalized $[E_9]$ cluster to be synthesized in this way,[24a] and the alkylated analogues $[R\text{-}(Ge_9)_2\text{-}R]^{n-}$ (R = ^{t}Bu, ^{s}Bu, ^{n}Bu, ^{t}Am) have subsequently been accessed through the reaction of $[Ge_9]^{4-}$ with alkyl halides RX.[25a] Recent studies have shown that such substituted clusters can further react with various reagents, to generate products such as $[AuGe_{18}\{Si(SiMe_3)_3\}_6]^-$,[27a] $[Ge_9\{Si(SiMe_3)_3\}_3(R)]$ (R= Tl, $SnPh_3$, Et), $[(Ph_3P)PdGe_9\{Si(SiMe_3)_3\}_3Et]$[28] and $[Pd_3Ge_{18}(E^iPr_3)_6]^{2-}$ (E = Si, Sn).[29] In marked contrast, reactions of the endohedral clusters, $[M@E_9]^{n-}$, with organometallic reagents are relatively rare,[14b] although it has been shown that metal-centered $[M@E_9]^{n-}$ fragments can act as ligands, for example in the clusters $[(Ni@Ge_9)(NiL)]^{x-}$,[7] $[(Ni@Ge_9)Pd(PPh_3)]^{2-}$,[8] $[(Ni@Sn_9)(Ni(CO)]^{3-}$,[30] $[Pt@Sn_9Pt(PPh_3)]^{2-}$,[30] $[Pd@Sn_9Pd(SnCy_3)]^{3-}$,[31] and $[Ni@Sn_9Tl]^{3-}$.[14b] The majority of these clusters were obtained from one-pot reactions using the $[E_9]^{4-}$ ions as precursors, so it is not clear whether the encapsulation of a metal atom into the E_9 occurs before or after the coordination of the M-L fragment. In some cases, however, the encapsulation can be performed in a separate step, as for example in the formation of $[Ni@Ge_9Pd(PPh_3)]^{2-}$ from the reaction of $[Ge_9Pd(PPh_3)]^{3-}$ with $Ni(PPh_3)_4$. Metal-centered $[M@E_9]^{n-}$ clusters can also be obtained by direct extraction from ternary intermetallic phases, and this provides a solid platform for further reactivity studies.[14c, 17c, 32] For example, extraction of an ethylenediamine (en) solution of the ternary K-Co-Sn phase has been shown to give high yields of the clus-

ter $[Co@Sn_9]^{4-}$ which incorporates a d^9 metal atom.[19c, 32] In this contribution, we use the K-Co-Sn phase as a precursor to investigate directly the reactivity of the $[Co@Sn_9]^{4-}$ cluster with various transition metal fragments. Specifically, we report the synthesis and structures of four new clusters, $[Co@Sn_9Ni(CO)]^{3-}$ (**2**), $[Co@Sn_9Ni(C_2H_4)]^{3-}$ (**3**), $[Co@Sn_9Pt(PPh_3)]^{3-}$ (**4**), and $[Co@Sn_9AuPh]^{3-}$ (**5**), which constitute a new family of ternary functionalized Zintl clusters incorporating a Co atom. All clusters were also characterized by electrospray mass spectrometry and their electronic structure is explored using density functional theory.

Experimental Section

General Synthetic Methods. All manipulations and reactions were performed in a nitrogen atmosphere using standard Schlenk or glovebox techniques. The intermetallic precursors, $K_5Co_3Sn_9$, were synthesized according to previously reported procedures from stoichiometric mixtures of the elements (K: 99.95%, Aldrich; Sn: 99.8%, Strem, Co: 99.95%) heated to 1000 °C for 72 h in sealed niobium containers. [2.2.2]-crypt (4,7,13,16,21,24-hexaoxa-1,10-diazabicyclo [8.8.8]hexacosane, purchased from Sigma-Aldrich, 98%) was dried under vacuum for one day prior to use. $Au(PPh_3)Ph$ was prepared according to a literature procedure.[33] $Ni(COD)_2$ (COD= cyclooctadiene) (Strem, 98%), $Pt(PPh_3)_4$ (Alfa-Aesar, 98%) and $Ni(PPh_3)_2(CO)_2$ (Alfa-Aesar, 98%) were used as received after careful drying under vacuum. Ethylenediamine (en) (Aldrich, 99%), N,N-Dimethylformamide (DMF) and Acetonitrile (MeCN) were freshly distilled over CaH_2 prior to use. Toluene (tol) (Aldrich, 99.8%) was distilled from sodium/benzophenone under dinitrogen and stored under dinitrogen.

X-ray crystal structure determination. Suitable crystals were selected for single-crystal X-ray diffraction analyses. Crystallographic data were collected on a Bruker Apex II CCD diffractometer with graphite-monochromated Mo Kα radiation (λ = 0.71073 Å). Data processing was accomplished with the SAINT program. Structures were solved using direct methods (SHELXT，Olex2) and then refined using SHELXL-2014 and Olex2 to convergence, [34] in which all of the non-hydrogen atoms were refined anisotropically. Nonhydrogen atoms were refined with anisotropic displacement parameters during the final cycles. All hydrogen atoms of the organic molecule were placed by geometrical considerations and were added to the structure factor calculation. The crystal of **4** was refined as a 2-component inversion twin: the twin law (-1, 0, 0, 0, -1, 0, 0, 0, -1) gives a final refined BASF parameter of 0.319(7). Rotational disorder was found in one cluster site in compound **4** and this was modeled accordingly (see the Supporting Information for details). Non-merohedral twinning in the crystal **5** was identified [Twin Rot Mat within PLATON (Spek, 2009)][34c] and the crystal was refined with hkl 5 format. The twin law gives a final refined BASF parameter of 0.213(3). A summary of the crystallographic data for these five complexes is listed in Table 1. Selected bond distances and angles are given in Tables S1-S5. CCDC 1579015-1579019 contains the supplementary crystallographic data for this paper.

Powder X-Ray Diffraction. Phase analyses of precursors with nominal compositions $K_5Co_3Sn_9$ were carried out using a MiniFlex 600 X-ray powder diffractometer equipped with a Cu sealed tube (λ = 1.541 78 Å) at 40 kV and 40 mA. The products were finely ground in an agate mortar and filled into airtight tube.

Mass Spectrometry. Electrospray ionization mass spectrometry (ESI-MS) was performed in negative-ion mode on an LTQ linear Ion Trap Spectrometer. The spray voltage was 5.48 kV and the capillary temperature was kept at 300 °C. The capillary voltage was 30V. The samples were made up inside a glovebox under an inert atmosphere and rapidly transferred to the spectrometer in an air-tight syringe by direct infusion with a Harvard syringe pump at 15 uL/ min.

EPR Measurements: EPR spectra were acquired on a JEOL JES-FA200 EPR spectrometer. Experiments were conducted at room temperature using solid microcrystalline samples of the compound $K[K(2,2,2\text{-crypt})]_3[Co_{0.870(4)}@Sn_9]$ (**1**) with 1 mW microwave power, 0.1mT modulation amplitude, and a modulation frequency of 100 kHz.

Synthesis of $[K(2,2,2\text{-crypt})]_3[Co@Sn_9Ni(CO)]$•DMF $K_5Co_3Sn_9$ (140 mg, 0.1 mmol) and 2,2,2-crypt (100 mg, 0.406 mmol) were dissolved in en (2 mL) in a test tube and stirred for 30 min before addition of $Ni(PPh_3)_2(CO)_2$ (120 mg, 0.228 mmol). This solution was then stirred for 3 h before removal of en under vacuum. The residue was redissolved in DMF, after which the resulting dark-red solution was stirred for an additional 2 h and was then centrifuged and filtered. The resulting solution was layered with toluene. Large, dark-red block-shaped crystals were obtained after 3 days (60% crystalline yield, based on employed $K_5Co_3Sn_9$).

Synthesis of $[K(2,2,2\text{-crypt})]_3[Co@Sn_9Ni(C_2H_4)]$•en. $K_5Co_3Sn_9$ (140 mg, 0.1 mmol) and 2,2,2-crypt (100 mg, 0.406 mmol) were dissolved in en (2 mL) in a test tube. After 30 minutes $Ni(COD)_2$ (77 mg, 0.120 mmol) were added directly to the solution. The mixture was stirred for 3h making a dark solution. This solution was then stirred for 3 h at room temperature, after which the resulting brown solution was filtered, and then carefully layered by toluene to allow for crystallization. Dark block crystals crystallized after a one week. (25% crystalline yield, based on employed $K_5Co_3Sn_9$).

Table 1. Crystallographic data and structure refinement parameters for **2-5**

Compound	Compound **2**	Compound **3**	Compound **4**	Compound **5**
Empirical formula	$C_{58}H_{110}O_{20}N_7K_3CoNiSn_9$	$C_{60}H_{120}O_{18}N_8K_3CoNiSn_9$	$C_{79}H_{122}O_{18}N_6K_3PCoPtSn_9$	$C_{63}H_{119}O_{19}N_7K_3CoAuSn_9$
F_w	2528.67	2520.94	2914.51	2720.05
Crystal system	Triclinic	Triclinic	Monclinic	Monclinic
Space group	*P*-1	*P*-1	$P2_1$	$P2_1/c$
a/Å	15.5281(9)	14.2337(6)	16.0201(14)	14.144(2)
b/Å	15.9512(8)	15.2306(7)	23.727(2)	20.923(3)
c/Å	19.5119(10)	22.0075(9)	28.278(2)	32.590(4)
α/°	88.2524(11)	95.8280(10)	90	90
β/°	81.6378(12)	100.3020(10)	105.322(2)	107.535(5)
γ/°	72.4693(11)	96.8570(10)	90	90
V/ Å^3	4559.0(4)	4623.4(3)	10366.7(15)	9196(2)
Z	2	2	2	4
F(000)	2458	2452.0	5638	5244
ρ_{calcd} (g/cm^3)	1.842	1.808	1.868	1.137
μ (Mo Kα)/ mm^{-1}	2.994	2.950	3.822	4.358
R_1/wR_2 ($I > 2\sigma(I)$) [a]	0.0523/0.1403	0.0555/0.1426	0.0475/0.1118	0.1144/0.2789
R_1/wR_2 (all data)	0.0824/ 0.1663	0.0840/0.1567	0.0564/0.1174	0.1392/0.2872

Synthesis of [K(2,2,2-crypt)]$_6$[Co@Sn$_9$Pt(PPh$_3$)]$_2$. $K_5Co_3Sn_9$ (140 mg, 0.1 mmol) and 2,2,2-crypt (100 mg, 0.406 mmol) were dissolved in en (2 mL) in a test tube and allowed to stir for approximately 30 min before addi-tion of $Pt(PPh_3)_4$ (120 mg, 0.228 mmol). The reaction mixture was stirred for 3 h, after which the resulting dark-red solution was filtered and then layered with toluene to allow for crystallization. Large block-shaped crystals suitable for single crystal X-ray diffraction were obtained after 5 days (30% crystalline yield, based on the amount of $K_5Co_3Sn_9$ used).

Synthesis of [K(2,2,2-crypt)]$_3$[Co@Sn$_9$AuPh]. $K_5Co_3Sn_9$ (140 mg, 0.1 mmol) and 2,2,2-crypt (100 mg, 0.406 mmol) were dissolved in en (2 mL) in a test tube and allowed to stir for approximately 30 min before addition of $Au(PPh_3)Ph$ (120 mg, 0.228 mmol). This resulting dark brown solution was then stirred for 3 h before removal of en under vacuum. The residue was washed with toluene followed by dissolution in 3 mL DMF. The resulting dark-red solution was filtered, and then carefully layered by toluene to allow for crystallization. Large, dark-red block-shaped crystals suitable for single crystal X-ray diffraction were obtained after 3 days (35% crystalline yield, based on the amount of $K_5Co_3Sn_9$ used).

Quantum chemical investigations. DFT calculations were performed with Amsterdam Density Functional package(ADF2016.105)[35] using the PBE functional[36] along with Slater type basis sets of triple-ζ quality (TZP) on Au/Ni/Co/Sn and DZP on C/O/H.[37] The scalar relativistic zeroth-order regular approximation (ZORA) to the Dirac equation is used in all calculations.[38] The effect of the counterions was modeled by the Conductor-like Screening Model (COSMO) with default parameters.[39] The geometries were fully optimized, and confirmed to be local minima by the absence of imaginary vibrational frequencies. ¯Frequencies are calculated numerically.[40] The topology of the electron density was analyzed using Atoms in Molecules (AIM) theory.[41,42]

Results and Discussion

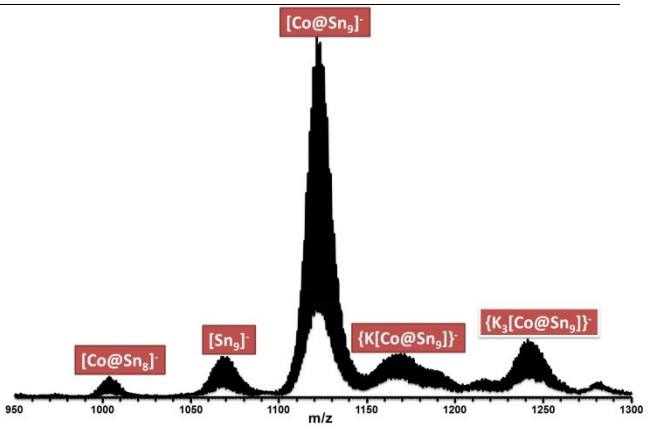

Figure 1. The electrospray mass spectrum (m/z: 950-1300) of "$K_5Co_3Sn_9$"/en in negative ion mode.

Following the synthetic strategy leading to "$K_{4.79}Co_{0.79}Sn_9$" reported by Fässler *et al*.,[19c, 32] the precursor with nominal composition "$K_5Co_3Sn_9$" was prepared by fusion of stoichiometric ratios of the elements at 1000 °C for 72 h. Powder X-ray diffraction measurements revealed that the "$K_5Co_3Sn_9$" phase is different from the $K_{4.79}Co_{0.79}Sn_9$ [19c, 32b] and $K_{12.95}Co_{0.95}Sn_{17}$ [32a] phases reported previously (Figure S1). Neither elemental Co nor any Co-Sn binary phase was observed. The precursor dissolved readily in en, resulting in an intensely colored dark solution. Upon layering with toluene, the solution yielded crystals of the known compound of $K[K(2,2,2\text{-crypt})]_3[Co_{0.870(4)}@Sn_9]$ in very high yields after a few days. [32b] The cluster anion in this compound is a solid solution of $[Co@Sn_9]^{4-}$ and empty $[Sn_9]^{4-}$, and crystallographic refinement revealed a defect on the Co position with site occupation of about 0.870(4), which differs only slightly from the 0.677(2) site occupation for the Co position in the compound $K[K([2.2.2]crypt)]_3[Co_{0.677(2)}@Sn_9]$ reported by Fässler *et al*. [32b]. The structure of **1** is a distorted mono-capped square antiprism with *pseudo-*C_{4v} symmetry. The $[Co@Sn_9]^{4-}$ ion is a nine-vertex, 21-electron, cluster and adopts a *nido* structure.

The paramagnetic character of **1** was corroborated by EPR spectroscopy (Figure S2). Further inspection of the "$K_5Co_3Sn_9$"/en solutions by ESI-MS shows that the spectrum is dominated by the $[Co@Sn_9]^-$ species (Figure 1 and Figure S4), indicating that cluster **1** is readily formed upon simple dissolution of the precursor in en. Note also that the empty $[Sn_9]^-$ species is present only in very small amounts.

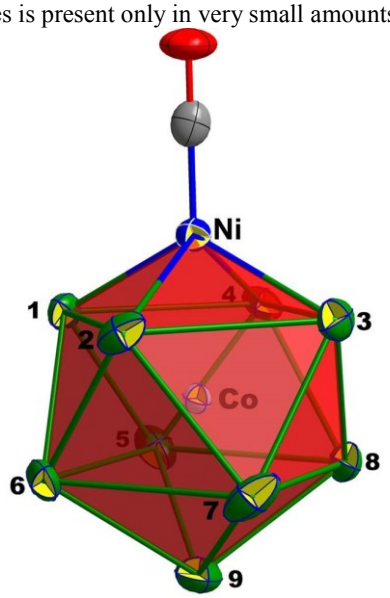

Figure 2. View of the geometry of $[Co@Sn_9Ni(CO)]^{3-}$ cluster, a bi-capped square antiprism. (Drawn at 50% probability).

Structure of $[Co@Sn_9Ni(CO)]^{3-}$ (2) The reactions of transition metal based organometallic compounds with **1** were investigated using "$K_5Co_3Sn_9$" as the precursor material. A solution of "$K_5Co_3Sn_9$" in en reacts with $Ni(PPh_3)_2(CO)_2$ to give the trimetallic anion **2**, crystals of which were obtained with 2,2,2-crypt as a cation-sequestering agent. The structures obtained in this way suffered from extensive disorder, but high-quality crystals of $[K(2,2,2\text{-crypt})]_3[Co@Sn_9Ni(CO)]\cdot DMF$ suitable for single crystal diffraction were finally recrystallized from a DMF solution layered with toluene. The trimetallic anion adopts a bi-capped square antiprismatic structure with one capping vertex occupied by a Ni-CO fragment (Figure 2). **2** is structurally very similar to the known species $[Ni@Sn_9Ni(CO)]^{3-}$ which has one more electron,[30] and is also virtually C_{4v}-symmetric with a regular mono-capped square anti-prismatic $NiSn_9$ core. The Sn–Sn contacts along the edges of the polyhedron of **2** fall in the range 2.888(9) to 3.445(9) Å, comparable to those in **1**. The longest Sn-Sn contacts occur within the two square faces Sn_1 to Sn_4 (av. 3.279 (2) Å) and Sn_5 to Sn_8 (av. 3.400(2) Å). The distances from the centered Co to the Sn atoms range from 2.637 to 2.745 Å, the longest being to the apical Sn atom, and they compare favorably with those in both $[Co@Sn_9]^{4-}$ and $[Co_2@Sn_{17}]^{5-}$.[19c] The distances from the capping nickel to the four adjacent Sn atoms fall in a very narrow range from 2.618 to 2.643 Å while the Co-Ni bond length is 2.501(8) Å, somewhat longer than that in the organometallic complex $CoNi_2(\eta^5\text{-}C_5H_5)_3(\mu_3\text{-}CO)_2$ (av. 2.38 Å),[43] but similar to that anionic clusters such as $[Ni_9CoC_2(CO)_{16-x}]^{3-}$ (x = 0, 1) (av. 2.53 Å).[44] The C-O bond length is 1.183 Å and the carbonyl region of the IR spectrum shows a C-O stretching mode at 1832 cm^{-1} (Figure S3), similar to the value of 1851 cm^{-1} observed in isoelectronic $[Ni@Sn_9Ni(CO)]^{3-}$.[30] The relatively low frequencies in these two clusters suggest strong back-donation from the electron-rich cluster to the Ni atom, and subsequently to the CO π* orbitals of the carbonyl ligand.[45]

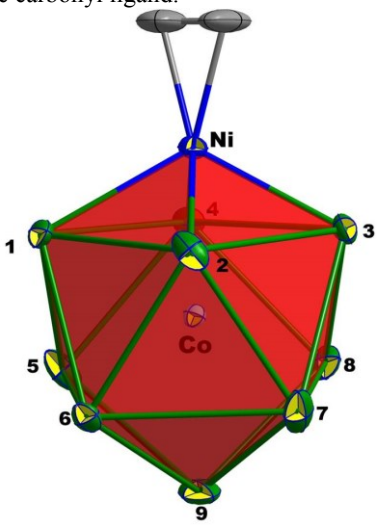

Figure 3. View of the geometry of $[Co@Sn_9Ni(C_2H_4)]^{3-}$ cluster. (Drawn at 50% probability).

Structure of $[Co@Sn_9Ni(C_2H_4)]^{3-}$ (3) An analogous reaction was carried out with $Ni(COD)_2$ in en solution, from which the cluster $[Co@Sn_9Ni(C_2H_4)]^{3-}$ was isolated as its $[K(2,2,2\text{-crypt})]^+$ salt in low yield. As shown in Figure 3, **3** is a bi-capped square antiprism where the Ni atom is one of the two capping vertices. The formation of **3** can therefore be viewed as the attachment of a neutral $Ni(C_2H_4)$ fragment to the open square face of C_{4v}-symmetrc $[Co@Sn_9]^{4-}$. The Co-Ni bond length of 2.525(10) Å in **3** is very similar to that in **2**, 2.501(8) Å, but in marked contrast to **2**, the geometry of the $[Co@Sn_9]$ core in **3** is distorted by a substantial elongation of the Sn5-Sn8 contact, from 3.504(8) in **1** to 3.903(13) Å) in **3**. In addition, whilst the Sn9-Co-Ni unit is almost linear in in **2**, it is distinctly bent in **3** (170.36°). As a result, the Ni-Sn distances to the four atoms of the capped square vary more widely in **3** than in **2**, from 2.563(8) Å (Ni1-Sn4) to 2.779(12) Å (Ni1-Sn2). The Co-Sn contacts within the square antiprism (2.575(14)-2.692(13) Å) are similar to those in **1** (2.567(1)-2.610(1) Å), while the Co-Sn9 distance is somewhat shorter (2.704(1) Å in **1** vs 2.745(1) Å in **2**).

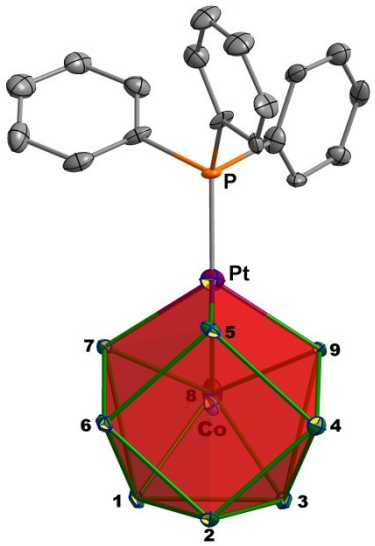

Figure 4. View of the geometry of the $[Co@Sn_9Pt(PPh_3)]^{3-}$ cluster, a cobalt centered tricapped trigonal prism where one of the triangular faces is capped by a Pt-PPh_3 fragment. (Drawn at 50% probability).

Structure of $[Co@Sn_9Pt(PPh_3)]^{3-}$ (4) Cluster **4** was obtained from the reaction of an en solution of "$K_5Co_3Sn_9$" with $Pt(PPh_3)_4$. The $[K(2,2,2\text{-crypt})]^+$ salt of **4** is monoclinic (space group $P2_1$) and contains two independent cluster sites in the asymmetric unit. One is well behaved and the other exhibits rotational disorder which was modeled accordingly (Figure S4). Only the structural properties of the well behaved cluster are discussed here. Cluster **4** is a pseudo-C_{3v} symmetric distorted tricapped trigonal prism with a $CoSn_9$ core capped by a Pt-PPh_3 fragment on top of one triangular face (Figure 4). It is isostructural with the previously reported analogues $[Pt@Sn_9Pt(PPh_3)]^{3-}$, $[Pd@Sn_9Pd(SnCy_3]^{3-}$ and $[Ni@Ge_9NiL]^{x-}$, L = CO, en. The coordination of $[CoSn_9]^{4-}$ by Pt-PPh_3 fragment therefore causes a rearrangement of the $CoSn_9$ core from the C_{4v}–symmetric mono-capped square antiprism common to **1**, **2** and **3** to the *pseudo*-C_{3v} distorted tricapped trigonal prism of **4**. The three Pt-Sn distances in **4** lie in a very narrow range of 2.655(10)–2.666(8) Å. The triangular Sn7-8-9 face is expanded (average Sn-Sn distances 3.95 (2) Å), as is the Sn2-Sn5 prism edge (3.950(1) Å). The remaining Sn-Sn bonds within the cluster are in the range 2.907 (7)-3.204 (11) Å, similar to those in both $[Pt@Sn_9Pt(PPh_3)]^{3-}$ [30] and $[Pd@Sn_9Pd(SnCy_3]^{3-}$. [31] The 10-vertex cluster is approximately spherical, with all distances from the central Co to Sn or Pt falling in the range of 2.585(15)-2.725(5) Å. The Co-Pt bond length is 2.608(10) Å, slightly shorter than those in the cluster $[Co_8Pt_4C_2(CO)_{24}]^{2-}$ (av. 2.71 Å).[46]

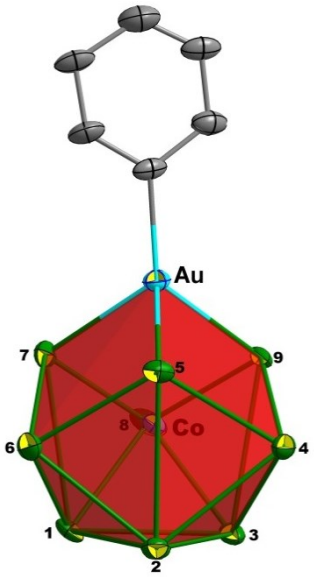

Figure 5. View of the geometry of the $[Co@Sn_9AuPh]^{3-}$ cluster. (Drawn at 50% probability).

Structure of $[Co@Sn_9AuPh]^{3-}$ (5) $[Co@Sn_9AuPh]^{3-}$ was obtained by a similar reaction of $Au(PPh_3)Ph$ with "$K_5Co_3Sn_9$" in en solution. The shape of **5** (Figure 5) resembles that of **4**: a cobalt-centered, tri-capped trigonal prism with the Au-Ph fragment capping an open trigonal prismatic base. **5** is the first reported example of an Au-Ph fragment bound to a Zintl cluster. As in **4**, the Au-Sn contacts are almost identical (2.727(10)-2.742(8) Å) and the Sn–Sn bonds on the capped face are expanded (the Sn5-Sn7, Sn7-Sn9 and Sn9-Sn5 separations are 3.933(8), 3.999(4) and 3.968(3) Å, respectively). The remaining Sn-Sn distances fall in the range 2.923(8)-3.407(8) Å. The central trigonal prism in **5** is regular with three prismatic edges fall in the range of 3.322(8)- 3.407(8) Å. The cluster is again approximately spherical, with a Co-Au distance of 2.678 Å, slightly shorter than the average 2.718(3) Å in the cluster $Co_6C(CO)_{12}(AuPPh_3)_4$.[47] Co-Sn distances lie in the normal range, 2.570(8) and 2.766(8).

ESI-MS Studies The four new compounds **2-5** described above all dissolve readily in CH_3CN, and their ESI-MS spectra were recorded from solution in negative ion mode. Due to the presence of multiple Sn isotopes, all cluster-based peaks in the spectrum appear as distinct mass envelopes, which facilitate a clear assignment of signals. As is usually the case for negative ion mode ESI-MS studies of anionic Zintl species, the spectrum shows only mono-anionic clusters due to the oxidation of parent species with more negative charge during ionization. As shown in Figures 6 and 7, the negative ion mode spectra of the four compounds feature mass envelopes corresponding to $[CoSn_9ML]^-$ (m/z= 1214.02, 1214.06, 1584.68 and 1460.08 for **1**, **2**, **3** and **4**, respectively), along with peaks corresponding to the ion-paired components $\{[K(2,2,2\text{-crypt})][CoSn_9ML)]\}^-$ (m/z = 1629.02, 1629.12 and 1816.98

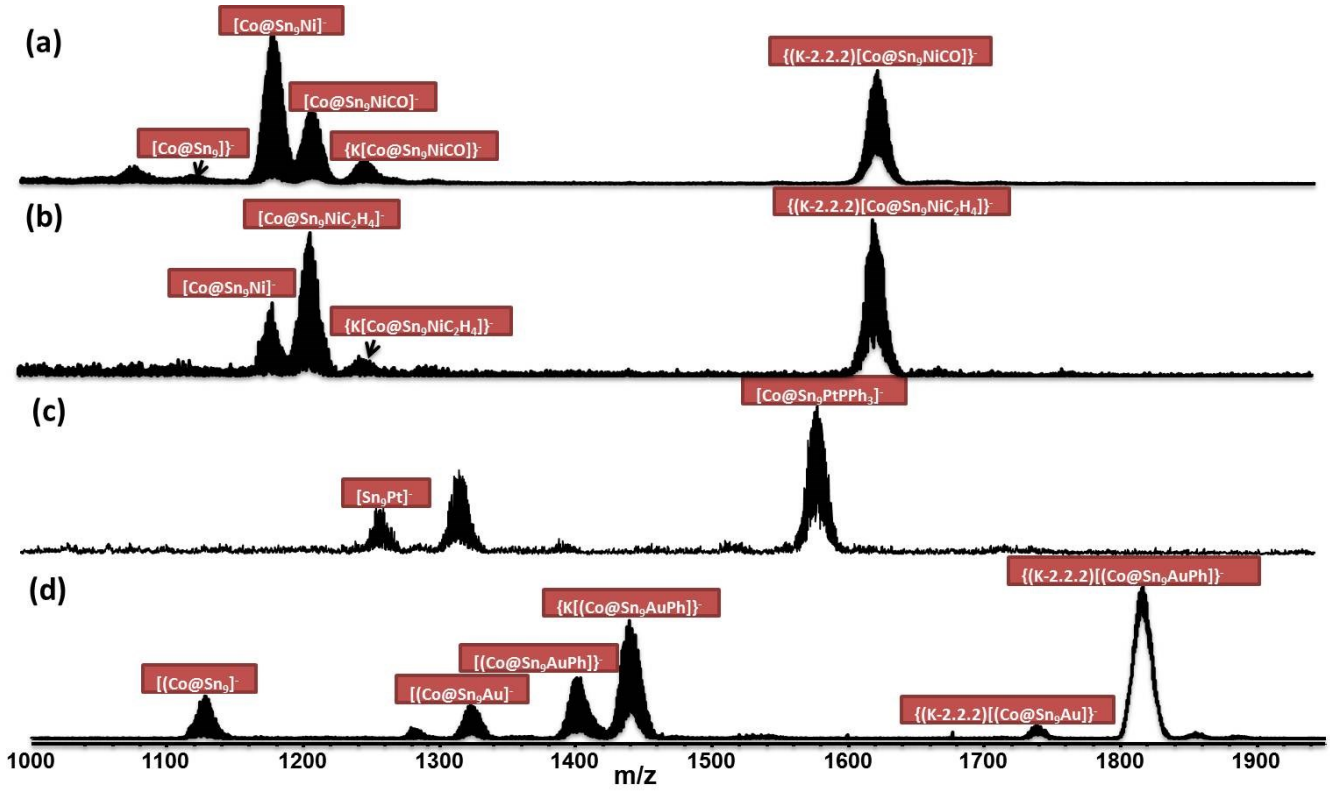

Figure 6. The full electrospray mass spectrum (m/z: 1000 – 2000) in negative ion mode of the CH_3CN solution containing **2–5**. Mass envelopes correspond to: (a) $[K(2,2,2\text{-crypt})]_3[Co@Sn_9Ni(CO)]\bullet DMF$, (b) $[K(2,2,2\text{-crypt})_{]3}[Co@Sn_9Ni(C_2H_4)]\bullet en$, (c) $[K(2,2,2\text{-crypt})]_6[Co@Sn_9Pt(PPh_3)]_2$ and (d) $[K(2,2,2\text{-crypt})]_3[Co@Sn_9AuPh]$.

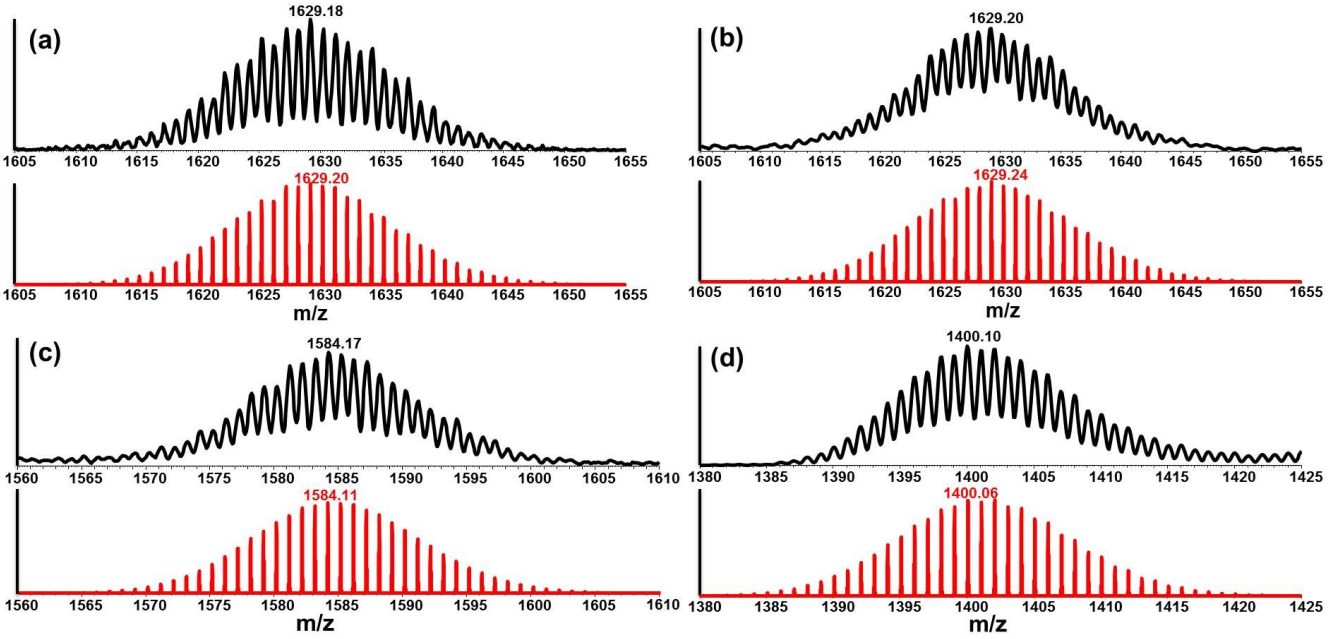

Figure 7. Selected negative ion-mode electrospray mass-envelope corresponding to $\{[K(2,2,2\text{-crypt})][Co@Sn_9NiCO]\}^-$ (a), $\{[K(2,2,2\text{-crypt})][Co@Sn_9Ni(C_2H_4)]\}^-$ (b), $[Co@Sn_9Pt(PPh_3)]^-$ (c) and $[Co@Sn_9AuPh]^-$ (d). Recorded experimental data are given in black with calculated isotopic distributions in red.

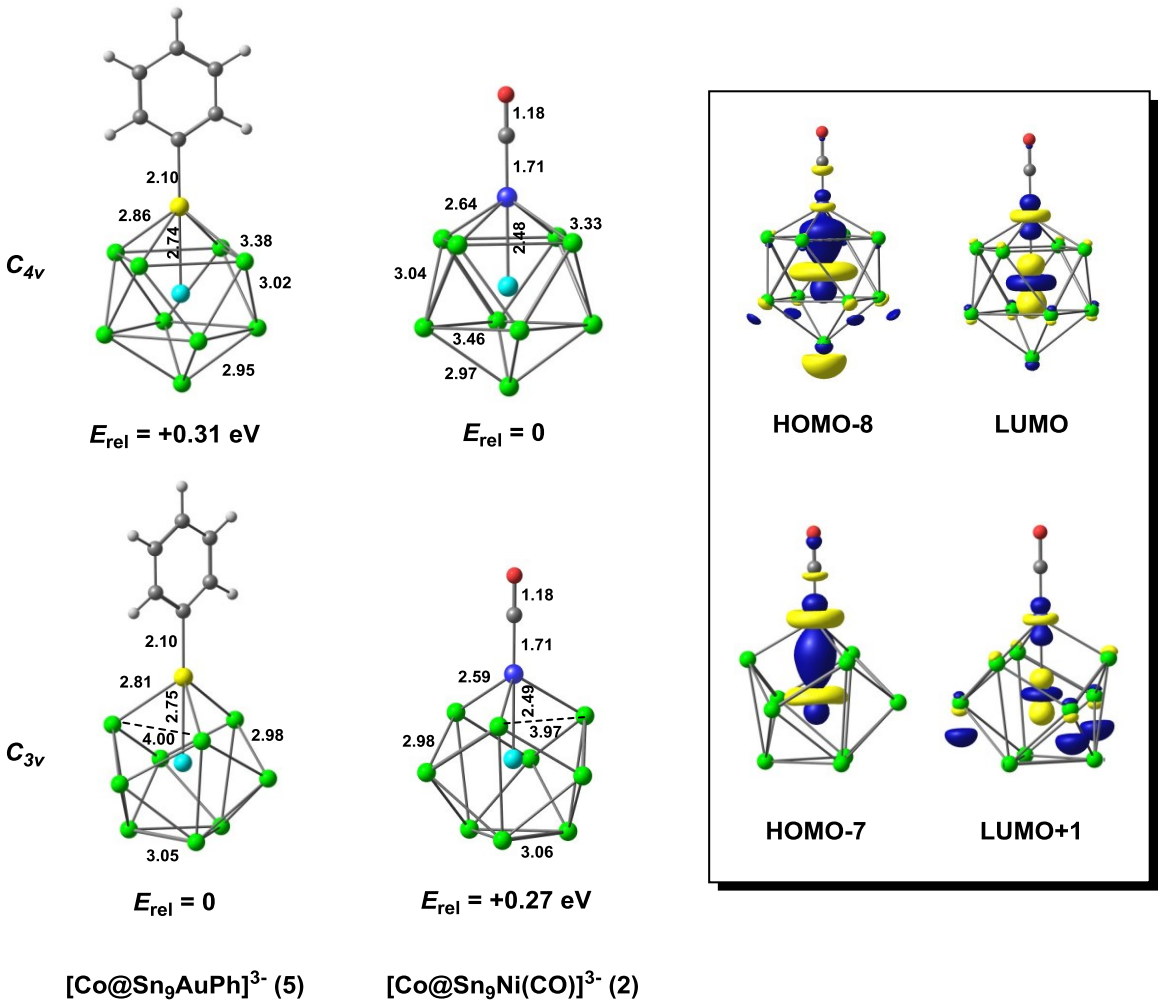

Figure 8. Optimized structures of the C_{4v} and C_{3v} isomers of $[Co@Sn_9AuPh]^{3-}$ (**5**) and $[Co@Sn_9Ni(CO)]^{3-}$ (**2**). Inset: selected frontier Kohn-Sham orbitals of the two isomers of **2**.

for **2**, **3** and **5**, respectively) and $\{K[CoSn_9ML)]\}^-$ (m/z = 1253.12, 1253.16, and 1440.49 for **2**, **3** and **5**, respectively). In addition, peaks arising from cluster derivatives after loss of the organic fragments were also detected, *i.e.*, $CoSn_9Ni$, and $CoSn_9Au$, $[CoSn_9M]\}^-$ at m/z = 1186.01 and 1324.28, respectively (Figures S16 and S20). Weak signals for $[Co@Sn_9]^-$ and $\{[K(2,2,2\text{-crypt})][CoSn_9Au]\}^-$ (Figure S23) were also observed.

Computational Studies (DFT). The structures of clusters **2** and **5** have been optimized using density functional theory (PBE with TZP basis sets on Co/Sn/Ni/Au and DZP basis sets on C/O/H), starting from geometries where the Sn_9 unit has either C_{4v} or C_{3v} symmetry (as in the crystal structures of **2** and **5**, respectively). In cluster **2** the overall symmetry of the molecule is then also C_{4v} or C_{3v}, but for **5**, the presence of the phenyl group reduces the overall symmetry to C_{2v} or C_s. Nevertheless, we refer to the two isomers as 'C_{4v}' and 'C_{3v}', respectively. In both clusters we have been able to locate distinct local minima corresponding to both C_{4v} and C_{3v}, shown in Figure 8. The relative energies of the two isomers are consistent with experiment, in so much as the C_{4v}-symmetric isomer is most stable for **2** while the C_{3v}-symmetric alternative is preferred for **5**. The differences in energy are, however, very marginal: $\Delta E = E(C_{4v}) - E(C_{3v}) = -0.27$ eV for **2** and +0.31 eV for **5**. The optimized structural parameters of the most stable isomer in each case are in excellent agreement with the available experimental data – computed Co-M , Co-Sn and M-Sn bond lengths are within 0.07 Å of the X-ray values in all cases. The presence or absence of a direct covalent bond between the endohedral Co and the capping metal (Ni or Au) is not easy to establish using the structural data in isolation, because the distance between the two atoms (2.501(8) Å and 2.718(3) Å for **2** and **5**, respectively), whilst short, is necessarily constrained by the dimensions of the Sn_9M cage. Nevertheless, the dominant Ni-Co σ* character in the LUMO of the more stable C_{4v}-symmetric isomer of **2**, shown in the inset in Figure 8, provides convincing evidence for the presence of such a bond. An analysis of the topology of the electron density using the Atoms in Molecules (AIM) approach (Supporting information, Figure S25) confirms the presence of a critical point between

the two transition metal atoms. Similar features emerge in both the Kohn-Sham orbitals and the electron densities of the C_{3v}-symmetric isomer, although the Co-Ni σ* character in the LUMO+1 is diluted, with greater contributions from orbitals on the Sn_9 fragment. Very similar patterns can also be identified in the two isomers of cluster **5** (see supporting information, Figure S26), leading us to conclude that Co-M bonding is a common feature of this family of clusters, irrespective of the identity of M or the geometry of the Sn_9 unit. We note that Eichhorn and co-workers also proposed the presence of a Pt-Pt bond in $[Pt@Sn_9Pt(PPh_3)]^{2-}$, although the details of the electronic structure were not discussed.[30]

A number of closely-related tin and germanium clusters have been reported in the literature, including $[Pt@Sn_9Pt(PPh_3)]^{2-}$,[30] $[Ni@Ge_9Pd(PPh_3)]^{2-}$,[8] and $[Ni@Ge_9NiL]^{x-}$ (L = PPh_3, en, CO, PhC ≡ C-),[7] all of which have distorted tricapped trigonal prismatic geometries similar to **4** and **5**, and C_{4v}-symmetric $[Ni@Sn_9Ni(CO)]^{3-}$.[30]

In their discussion of the electronic structure of $[Ni@Ge_9Ni(CO)]^{2-}$, Goicoechea and Sevov did not propose a Ni-Ni bond, instead formulating the cluster as a 20-electron $[Ge_9]^{2-}$ fragment which leaves both the endohedral and capping Ni atoms zero-valent with d^{10} configurations and therefore no metal-metal bond. The 20-electron count is apparently consistent with the presence of a tricapped trigonal prismatic Ge_9 unit, a *closo* structure, which would demand 2(n + 1) = 20 skeletal electrons according to Wade's rules. Our computational results suggest a rather different perspective on electron counting, in which the clusters have 22-valence electrons rather than 20, containing a $[Sn_9]^{4-}$ fragment and a bimetallic $[Co\text{-}M\text{-}L]^{+}$ unit with a $\{d^9d^9\}$ configuration and hence a Co-M σ bond. In effect, the two electrons in the Co-M σ* orbital are expelled from the Co-M unit, and are transferred to the Sn_9 fragment, raising its electron count to 22.

The argument for a $[Sn_9]^{4-}/\{d^9d^9\}$ resonance structure is most compelling for the C_{4v}-symmetric Sn_9 fragment in **2** and **3**, simply because the mono-capped square anti-prismatic architecture is the 'natural' geometry anticipated for a 22-electron $[Sn_9]^{4-}$ cluster (*i.e. nido*) The tri-capped trigonal prismatic architecture is, in contrast, the natural structure for a 20-electron $[Sn_9]^{2-}$ cluster (*closo*) but the same D_{3h}-symmetric architecture can support $[Ge_9]^{2-}$, $[Ge_9]^{3-}$ and $[Ge_9]^{4-}$ oxidation levels. Structurally, these differ primarily in the length of the trigonal edges, and it is significant, therefore, that the corresponding edges in **2** and **5** (3.43 Å and 3.38 Å, respectively) lie approximately midway between the computed values for isolated $[Sn_9]^{2-}$ and $[Sn_9]^{4-}$ clusters (3.22 Å and 3.67 Å, respectively). The structural data indicate that even in the C_{3v}-symmetric isomers, the negative charge on the Sn_9 fragment is greater than −2.

The $[Sn_9]^{4-}/\{d^9d^9\}$ and $[Sn_9]^{2-}/\{d^{10}d^{10}\}$ resonance structures clearly represent two limiting descriptions of the bonding in these clusters, and they are linked by a continuum of intermediate bonding situations. The position of a given cluster on the $[Sn_9]^{4-}/\{d^9d^9\}$ ↔ $[Sn_9]^{2-}/\{d^{10}d^{10}\}$ continuum is most easily defined by the character of the vacant orbital shown in Figure 8: more Sn_9 and less Co-M σ* character in the vacant orbital indicates a shift towards the $[Sn_9]^{2-}/\{d^{10}d^{10}\}$ limit. In this context, the greater Sn_9 character in the LUMO+1 of the C_{3v}-symmetric isomer of **2** noted previously is significant because it indicates that it lies closer to the $[Sn_9]^{2-}/\{d^{10}d^{10}\}$ limit than the C_{4v}-symmetric analogues. The relationship between the electron density distribution and the ground-state geometry of these clusters can be further demonstrated by considering a series which includes **2** and its (hypothetical) isostructural and isoelectronic analogues $[Co@Sn_9Cu(CO)]^{2-}$ and $[Co@Sn_9Zn(CO)]^{1-}$. Within this series, the increasing nuclear charge at the capping atom (Ni→Cu→Zn) should stabilize the Co-M σ* orbital, and so shift the balance from the $[Sn_9]^{4-}/\{d^9d^9\}$ limit towards $[Sn_9]^{2-}/\{d^{10}d^{10}\}$. As we move across this series we do indeed find an almost linear increase in the stability of the C_{3v} isomer over its C_{4v} alternative: $E(C_{4v})$ - $E(C_{3v})$ = –0.27 eV for **2**, $[Co@Sn_9Ni(CO)]^{2-}$, but only –0.05 eV for $[Co@Sn_9Cu(CO)]^{2-}$ and +0.12 eV for $[Co@Sn_9Zn(CO)]^{1-}$. The structure of a cluster is therefore intimately connected to its position on the $[Sn_9]^{4-}/\{d^9d^9\}$ ↔ $[Sn_9]^{2-}/\{d^{10}d^{10}\}$ continuum: a shift to the right causes a stabilization of the tri-capped trigonal prismatic structure relative to its mono-capped square anti-prismatic analogue. Based on this argument, it appears that the preference for the C_{3v}-symmetric isomer for both **4** and **5** is indicative of a weaker Co-M interaction and therefore a more stable Co-M σ* orbital when M is a 3rd row transition metal, which in turn drives a shift towards the $[Sn_9]^{2-}/\{d^{10}d^{10}\}$ limit.

Conclusions

In summary, we have presented here a systematic study of the reactivity of the $[Co@Sn_9]^{4-}$ anion with a range of transition metal reagents, using for the first time the "$K_5Co_3Sn_9$" phase as the precursor. The result is a family of functionalized Co-centered cluster anions, $[Co@Sn_9Ni(CO)]^{3-}$, $[Co@Sn_9Ni(C_2H_4)]^{3-}$, $[Co@Sn_9Pt(PPh_3)]^{3-}$ and $[Co@Sn_9AuPh]^{3-}$, each of which has been structurally characterized. The transition from a mono-capped square antiprismatic architecture for the Sn_9 unit (in **2** and **3**) to a tri-capped trigonal prismatic one (in **4** and **5**) can be understood in terms of a continuum between limiting $[Sn_9]^{4-}/\{d^9d^9\}$ and $[Sn_9]^{2-}/\{d^{10}d^{10}\}$ resonance forms. This new body of data clearly illustrates the great potential of the $[Co@Sn_9]^{4-}$ cluster, which can be extracted directly from K-Co-Sn phases in high yields, as a building block from which more complex structures can be constructed. We anticipate that the development of precursors other than $[E_9]^{n-}$ may open up a wealth of new possibilities in the field of Zintl cluster chemistry.

Author Information

Corresponding Author
*E-mail: szm@ciac.ac.cn; john.mcgrady@chem.ox.ac.uk
http://zhongmingsun.weebly.com/

Acknowledgements

We acknowledge the support of this work by National Natural Science Foundation of China (No. 21722106, 21571171) and Youth Foundation project of Jilin province 20180520009JH. We thank Dr. Ning Li for his help in the single crystal X-ray diffraction analyses. We also thank Dr. Jun-Peng Xing for his help with the ESI-Mass experiments.

REFERENCES

(1) (a) Fässler, T. F.; Hoffmann, S. D.; Endohedral Zintl ions: intermetalloid clusters, *Angew. Chem., Int. Ed.* **2004**, *43*, 6242–6247; (b) Scharfe, S.; Kraus, F.; Stegmaier, S.; Schier, A.; Fässler, T. F. Zintl ions, cage compounds, and intermetalloid clusters of group 14 and group 15 elements, *Angew. Chem. Int. Ed*. **2011**, *50*, 3630–3670 (c) Weinert, B.; Dehnen, S.; Binary and ternary intermetalloid clusters, *Struct. Bond*. **2017**, *174*, 99–134.; (d) N. Korber, *Angew. Chem. Int. Ed*., The Shape of germanium clusters to come, **2009**, *48*, 3216-3217

(2) (a) Moses, M. J.; Fettinger, J.; Eichhorn, B.; Charged molecular alloys: synthesis and characterization of the binary anions $Pd_7As_{16}^{4-}$ and $Pd_2As_{14}^{4-}$, *J. Am. Chem. Soc*. **2002**, *124*, 5944–5945; (b) Moses, M. J.; Fettinger, J. C.; Eichhorn, B. W. $[Ni_5Sb_{17}]^{4-}$ transition-metal Zintl ion complex: crossing the Zintl border in molecular intermetalloid clusters, *Inorg. Chem*. **2007**, *46*, 1036–1038; (c) Goicoechea, J. M.; Sevov, S. C. $[Zn_9Bi_{11}]^{5-}$: A ligand-free intermetalloid cluster, *Angew. Chem. Int. Ed*. **2006**, *45*, 5147–5150; (d) Moses, M. J.; Fettinger, J. C.; Eichhorn, B. W. Interpenetrating As_{20} fullerene and Ni_{12} icosahedra in the onion-skin $[As@Ni_{12}@As_{20}]^{3-}$ ion, *Science*. ***2003***, *300*, 778–780; (e) Wang, Y.; Moses-DeBusk, M.; Stevens, L.; Hu, J.; Zavalij, P.; Bowen, K.; Dunlap, B. I..; Glaser, E. R.; Eichhorn, B. W. $Sb@Ni_{12}@Sb_{20}^{-/+}$ and $Sb@Pd_{12}@Sb_{20}^{n}$ Cluster Anions, Where n = +1,−1, −3, −4: Multi-Oxidation-State Clusters of Interpenetrating Platonic Solids Onion-skin $[As@Ni_{12}@As_{20}]^{3-}$ Ion, *J. Am. Chem. Soc*. **2017**, *139*, 619–622.; (f) Wang, Y.; Zavaliji, P.; Eichhorn, B. $[(ZnSb_6)_2]^{4-}$: a new structure type of coupled norbornadienelike dimer, DOI: 10.1039/C7CC07454A.

(3) (a) Lips, F.; Clérac, R.; Dehnen, S. $[Eu@Sn_6Bi_8]^{4-}$: A mini-fullerane-type Zintl anion containing a lanthanide ion, *Angew. Chem. Int. Ed.* **2011**, *50*, 960–964; (b) Lips, F.; Hołyńska, M.; Clérac, R.; Linne, U.; Pöttgen, R.; Weigend, F.; Dehnen, S. Doped semimetal clusters: ternary, intermetalloid anions $[Ln@Sn_7Bi_7]^{4-}$ and $[Ln@Sn_4Bi_9]^{4-}$ (Ln = La, Ce) with adjustable magnetic properties, *J. Am. Chem. Soc*. **2012**, *134*, 1181–1191; (c) Lichtenberger, N.; Wilson, R. J.; Massa, W.; Clérac, R.; Weigend, F.; Dehnen, S. Main group metal–actinide magnetic coupling and structural response upon U^{4+} inclusion into Bi, Tl/Bi, or Pb/Bi cages, *J. Am. Chem. Soc*. **2016**, 138, 9033–9036; (d) Weinert, B.; Muller, F.; Harms, K.; Clérac, R.; Dehnen, S. Origin and location of electrons and protons during the formation of intermetalloid clusters $[Sm@Ga_{3-x}H_{3-2x}Bi_{10+x}]^{3-}$ (x=0, 1), *Angew. Chem. Int. Ed*. **2014**, *53*, 11979–11983; (e) Mitzinger, S.; Broeckaert, L.; Massa, W.; Dehnen, S. $[V@Ge_8As_4]^{3-}$ and $[Nb@Ge_8As_6]^{3-}$: encapsulation of electron-poor transition metal atoms, *Chem. Commun.* **2015**, *51*, 3866–3869; (f) Mitzinger, S.; Broeckaert, L.; Massa, W.; Weigend, F.; Dehnen, S. Understanding of multimetallic cluster growth, *Nat. Commun*. **2016**, *7*, 10480–10490; (g) Wilson, R. J.; Dehnen, S; $(Ge_4Bi_{14})^{4-}$: A Case of "Element Segregation" on the Molecular Level, *Angew. Chem. Int. Ed*. **2017**, 56, 3098–3102. (h) Mayer, K.; Dums, J. V.; Klein, W.; Fässler, T. F, $[SnBi_3]^{5-}$, A Carbonate Analogue Comprising Exclusively Metal Atoms, *Angew. Chem. Int. Ed*. **2017**, *56*, 15159–15163. (i) Wilson, R. J.; Broeckaert, L.; Spitzer, F.; Weigend, F.; Dehnen S; $\{[CuSn_5Sb_3]^{2-}\}_2$: A Dimer of Inhomogeneous Superatoms, *Angew. Chem. Int. Ed*. **2016**, *55*, 11775–11780

(4) Sevov, S. C.; Goicoechea, J. M. Chemistry of deltahedral Zintl ions, *Organometallics*. **2006**, *25*, 5678.

(5) (a) Eichhorn, B. W.; Haushalter, R. C. Synthesis and structure of *closo*-$Sn_9Cr(CO)_3^{4-}$: The first member in a new class of polyhedral clusters, *J. Am. Chem. Soc*. **1988**, *110*. 8704. (b) Eichhorn, B. W.; Haushalter, R. C.; *Closo*-$[CrPb_9(CO)_3]^{4-}$: a 100 year history of the nonaplumbide tetra-anion. *J. Chem. Soc. Chem.Commun*. **1990**, 937. (c) Kesanli, B.; Fettinger, J.; Eichhorn, B. W. The *closo*-$[Sn_9M(CO)_3]^{4-}$ Zintl ion clusters where M= Cr, Mo, W: two structural isomers and their dynamic behavior, *Chem. Eur. J*. **2001**, *7*, 5277–5285. (d) Campbell, J.; Mercier, H. P. A.; Franke, H.; Santry, D.; Dixon, D. A.; Schrobilgen, G. J. Syntheses, crystal structures, and density functional theory calculations of the *closo*-$[1\text{-}M(CO)_3(\eta^4\text{-}E_9)]^{4-}$ (E = Sn, Pb; M = Mo, W) cluster anions and solution NMR spectroscopic characterization of $[1\text{-}M(CO)_3(\eta^4\text{-}Sn_9)]^{4-}$ (M = Cr, Mo, W), *Inorg. Chem.* **2002**, *41*, 86–107. (f) Yong, L.; Hoffmann, S. D.; Fässler, T. F. Crystal structures of $[K(2.2.2\text{-crypt})]_4[Pb_9Mo(CO)_3]^-$ isolation of the novel isomers $[(\eta^5\text{-}Pb_9)Mo(CO)_3]^{4-}$ beside $[(\eta^4\text{-}Pb_9)Mo(CO)_3]^{4-}$, *Eur. J. Inorg. Chem.* **2005**, 3663–3669.

(6) Joseph, S.; Hamberger, M.; Mutzbauer, F.; Härtl, O.; Meier, M.; Korber, N. Chemistry with Bare Silicon Clusters in Solution: A Transition-Metal Complex of a Polysilicide Anion, *Angew. Chem. Int. Ed.* **2009**, **48**, 8770 –8772.

(7) Goicoechea, J. M.; Sevov, S. C.; Deltahedral germanium clusters: insertion of transition-metal atoms and addition of organometallic fragments, *J. Am. Chem. Soc*. **2006**, *128*, 4155–4161.

(8) Sun, Z. M.; Zhao, Y. F.; Li, J.; Wang, L. S. Diversity of functionalized germanium Zintl clusters: syntheses and theoretical studies of $[Ge_9PdPPh_3]^{3-}$ and $[Ni@(Ge_9PdPPh_3)]^{2-}$, *J Clust Sci*. **2009**, *20*, 601–609.

(9) (a) Wang, J. Q.; Stegmaier, S.; Wahl, B.; Fässler, T. F. Step-by-step synthesis of the endohedral stannaspherene $[Ir@Sn_{12}]^{3-}$ via the capped cluster anion $[Sn_9Ir(cod)]^{3-}$, *Chem. Eur. J*. **2010**, *16*, 1793–1798. (b) Scharfe, S.; Fässler, T. F, Varying bonding modes of the Zintl ion $[Ge_9]^{4-}$ in Cu^I complexes: syntheses and structures of $[Cu(\eta^4\text{-}Ge_9)(PR_3)]^{3-}$ (R = ^{i}Pr, Cy) and $[Cu(\eta^4\text{-}Ge_9)(\eta^1\text{-}Ge_9)]^{7-}$, *Eur. J. Inorg. Chem*. **2010**, 1207–1213.

(10) (a) Goicoechea, J. M.; Sevov, S. C.; Organozinc derivatives of deltahedral Zintl ions: synthesis and characterization of *closo*-$[E_9Zn(C_6H_5)]^{3-}$ (E = Si, Ge, Sn, Pb), *Organometallics,* **2006**, 25, 4530–4536. (b) Zhou, B.; Denning, M. S.; Jones, C.; Goicoechea, J. M. Reductive cleavage of Zn-C bonds by group 14 Zintl anions synthesis and characterization of $[E_9ZnR]^{3-}$ (E = Ge, Sn, Pb; R = Mes, ^{i}Pr), *Dalton Trans.* 2009, 1571–1578. (c) Zhou, B.; Denning, M. S.; Chapman, T. A. D.; Goicoechea, J. M. Coupling reactions of functionalized Zintl ions $[E_9Cd(C_6H_5)]^{3-}$ (E= Sn, Pb) with tributyltinhydride: synthesis and isolation of $\{Sn_9CdSn[(CH_2)_3CH_3]_3\}^{3-}$, *Inorg. Chem*, **2009**, *48*. 2899-2907.

(11) Benda, C. B.; Waibel, M.; Fässler, T. F.; On the Formation of

Intermetalloid Clusters: Titanocene(III)diammin as a Versatile Reactant Toward Nonastannide Zintl Clusters, *Angew. Chem. Int. Ed*. **2015,** 54, 522 –526

(12) (a) Cui, L. F.; Huang, X.; Wang, L. M.; Zubarev, D. Y.; Boldyrev, A. I.; Li, J.; Wang, L. S. Sn_{12}^{2-}: Stannaspherene, *J. Am. Chem. Soc*. **2006**, *128*, 8390-8391.; (b) Cui, L. F.; Huang, X.; Wang, L. M.; Li, J.; Wang, L. S. Pb_{12}^{2-}: Plumbaspherene, *J. Phys. Chem. A.* **2006**, 110, 10169-10172.; (c) Cui, L. F.; Huang, X.; Wang, L. M.; Li, J.; Wang, L. S.; Endohedral Stannaspherenes $M@Sn_{12}^{-}$: A Rich Class of Stable Molecular Cage Clusters, *Angew. Chem., Int. Ed.* **2007**, 46, 742-745.

(13) (a) Esenturk, E. N.; Fettinger, J.; Lam, Y. F.; Eichhorn, B. $[Pt@Pb_{12}]^{2-}$, *Angew. Chem. Int. Ed*. **2004**, *43*, 2132–2134; (b) Esenturk, E. N.; Fettinger, J.; Eichhorn, B. The Pb_{12}^{2-} and Pb_{10}^{2-} Zintl ions and the $M@Pb_{12}^{2-}$ and $M@Pb_{10}^{2-}$ cluster series where M = Ni, Pd, Pt, *J. Am. Chem. Soc*. **2006**, *128*, 9178–9186.

(14) (a) Goicoechea, J. M.; Sevov, S. C. $[(Ni\text{-}Ni\text{-}Ni)@(Ge_9)_2]^{4-}$: A linear triatamic Nickel filament enclosed in a dimer of nine-atom Germanium clusters, *Angew. Chem. Int. Ed*. **2005**, *44,* 4026–4028; (b) Rios, D.; Gillett-Kunnath, M. M.; Taylor, J. D.; Oliver, A. G.; Sevov, S. C. Addition of a Thallium vertex to empty and centered nine-atom deltahedral Zintl ions of Germanium and Tin, *Inorg. Chem*. **2011**, *50*, 2373–2377. (c) Gillett-Kunnath, M. M.; Paik, J. I.; Jensen, S. M.; Taylor, J. D.; Sevov, S. C. Metal-centered deltahedral Zintl ions: Synthesis of $[Ni@Sn_9]^{4-}$ by direct extraction from intermetallic precursors and of the vertex-fused dimer $[\{Ni@Sn_8(\mu\text{-}Ge)_{1/2}\}_2]^{4-}$, *Inorg. Chem*. **2011**, *50*, 11695–11701.

(15) Scharfe, S.; Fässler, T. F.; Stegmaier, S.; Hoffman, S. D.; Ruhland, K. $[Cu@Sn_9]^{3-}$ and $[Cu@Pb_9]^{3-}$: intermetalloid clusters with endohedral Cu atoms in spherical environments, *Chem. Eur. J.* **2008**, *14*, 4479–4483.

(16) Esenturk, E. N.; Fettinger, J.; Eichhorn, B. The *closo*-Pb_{10}^{2-} Zintl ion in the $[Ni@Pb_{10}]^{2-}$ cluster, *Chem. Commun*. **2005**, 247–249.

(17) Zhou, B. B.; Kramer, T.; Thompson, A. L.; McGrady, J. E.; Goicoechea, J. M. A Highly Distorted Open-Shell Endohedral Zintl Cluster: $[Mn@Pb_{12}]^{3-}$, *Inorg. Chem.* **2011**, *50*, 8028–8037.

(18) (a) Liu, C; Popov, I, A.; Li, L. J.; Li, N.; Boldyrev, A. I.; Sun, Z. M; $[Co_2@Ge_{16}]^{4-}$: Localized vs. Delocalized Bonding in Two Isomeric Intermetalloid Clusters, *Chem. Eur.-J.* ***2017***, DOI: 10.1002/chem.201704444; (b) Jin, X.; Espinoza-Quintero, G.; Below, B.; Arcisauskaite, V.; Goicoechea, J. M.; McGrady, J. E., Structure and bonding in a bimetallic endohedral cage, $[Co_2@Ge_{16}]^{z-}$, J. Organomet. Chem., 2015, 792, 149-153.

(19) (a) Esenturk, E. N.; Fettinger, J. C.; Eichhorn, B. W. Synthesis, structure, and dynamic properties of $[Ni_2Sn_{17}]^{4-}$, *J. Am. Chem. Soc.* **2006**, *128*, 12−13. (b) Kesanli, B.; Halsig, J. E.; Zavalij, P.; Fettinger, J. C.; Lam, Y. F.; Eichhorn, B. W. Cluster growth and fragmentation in the highly fluxional Platinum derivatives of Sn_9^{4-}: synthesis, characterization, and solution dynamics of $Pt_2@Sn_{17}^{4-}$ and $Pt@Sn_9H^{3-}$, *J. Am. Chem. Soc*. **2007**, *129*, 4567−4574; (c) Hlukhyy, V.; He, H.; Jantke, L. A.; Fässler, T. F. The neat ternary solid $K_{5-x}Co_{1-x}Sn_9$ with endohedral $[Co@Sn_9]^{5-}$ cluster units: a precursor for soluble intermetalloid $[Co_2@Sn_{17}]^{5-}$ clusters, *Chem. Eur. J*. **2012**, *18*, 12000–12007.

(20) (a) Goicoechea, J. M.; Sevov, S. C. $[(Pd\text{-}Pd)@Ge_{18}]^{4-}$: a palladium dimer inside the largest single-cage deltahedron, *J. Am. Chem. Soc*. **2005**, *127*, 7676–7677. (b) Sun, Z. M.; Xiao, H.; Li, J.; Wang, L. S. $Pd_2@Sn_{18}^{4-}$: Fusion of two endohedral stannaspherenes, *J. Am. Chem. Soc*. **2007**, *129*, 9560–9561. (c) Kocak, F. S.; Zavalij, P.; Lam, Y. F.; Eichhorn, B. W. Solution dynamics and gas-phase chemistry of $Pd_2@Sn_{18}^{4-}$, *Inorg. Chem*. **2008**, *47*, 3515−3520.

(21) (a) Wang, J. Q.; Stegmaier, S.; Fässler, T. F. $[Co@Ge_{10}]^{3-}$: an intermetalloid cluster with archimedean pentagonal prismatic structure, *Angew. Chem. Int. Ed*. **2009**, *48*, 1998−2002;

(22) Zhou, B.; Denning, M. S.; Kays, D. L.; Goicoechea, J. M. Synthesis and isolation of $[Fe@Ge_{10}]^{3-}$: a pentagonal prismatic Zintl ion cage encapsulating an interstitial iron atom, *J. Am. Chem. Soc*. **2009**, *131*, 2802−2803.

(23) Espinoza-Quintero, G.; Duckworth, J. C. A.; Myers, W. K.; McGrady, J. E.; Goicoechea, J. M. Synthesis and characterization of $[Ru@Ge_{12}]^{3-}$: an endohedral 3-connected cluster, *J. Am. Chem. Soc*. **2014**, *136*, 1210−1213.

(24) (a) Ugrinov, A.; Sevov, S. C. $[Ph_2Bi{-}(Ge_9){-}BiPh_2]^{2-}$: a deltahedral Zintl ion functionalized by exo-bonded ligands, *J. Am. Chem. Soc*. **2002**, *124*, 2442−2443. (b) Ugrinov, A.; Sevov, S. C.; Derivatization of deltahedral Zintl ions by nucleophilic addition: $[Ph{-}Ge_9{-}SbPh_2]^{2-}$ and $[Ph_2Sb{-}Ge_9{-}Ge_9{-}SbPh_2]^{4-}$, *J. Am. Chem. Soc*. **2003**, 125, 14059−14064. (c) Ugrinov, A.; Sevov, S. C.; Rationally functionalized deltahedral Zintl ions: synthesis and characterization of $[Ge_9\text{-}ER_3]^{3-}$, $[R_3E\text{-}Ge_9\text{-}ER_3]^{2-}$, and $[R_3E\text{-}Ge_9\text{-}Ge_9\text{-}ER_3]^{4-}$ (E=Ge, Sn; R=Me, Ph), *Chem. Eur. J*. **2004**, *10*, 3727−3733. (d) Gillett-Kunnath, M. M.; Oliver, A. G.; Sevov, S. C. "n-doping" of deltahedral Zintl ions, *J. Am. Chem. Soc.* **2011**, *133*, 6560−6562. (e) Hansen, D. F.; Zhou, B.; Goicoechea, J. M. Further studies into the reactivity and coordination chemistry of $[Ge_9]^{4-}$ Zintl ions. The indium-containing anions $[In(Ge_9)_2]^{5-}$, $[(Ge_9)_2In(C_6H_5)]^{4-}$ and $[Ge_9\{In(C_6H_5)_3\}_2]^{4-}$, *J. Organomet. Chem*. **2012**, *721*, 53−61.

(25) (a) Hull, M. W.; Ugrinov, A.; Petrov, I.; Sevov, S. C. Alkylation of Deltahedral Zintl Clusters: Synthesis of $[R{-}Ge_9{-}Ge_9{-}R]^{4-}$ (R = ^{t}Bu, ^{s}Bu, ^{n}Bu, ^{t}Am) and Structure of $[^{t}Bu{-}Ge_9{-}Ge_9{-}^{t}Bu]^{4-}$, *Inorg. Chem.* **2007**, *46*, 2704−2708. (b) Hull, M. W.; Sevov, S. C. Addition of alkenes to deltahedral Zintl clusters by reaction with alkynes: synthesis and structure of $[Fc\text{-}CH{=}CH\text{-}Ge_9\text{-}CH{=}CH\text{-}Fc]^{2-}$, an organo-Zintl–organometallic anion, *Angew. Chem. Int. Ed*. **2007**, *46,* 6695−6698;. (c) Hull, M. W.; Sevov, S. C. Organo-Zintl clusters soluble in conventional organic solvents: setting the stage for organo-Zintl cluster chemistry, *Inorg. Chem*. **2007**, *46*, 10953−10955. (d) Chapman, D. J.; Sevov, S. C. Tin-based organo-Zintl ions: alkylation and alkenylation of Sn_9^{4-}, *Inorg. Chem*. **2008**, *47*, 6009−6013. (e) Hull, M. W.; Sevov, S. C. Functionalization of nine-atom deltahedral Zintl ions with organic substituents: detailed studies of the reactions, *J. Am. Chem. Soc*. **2009**, *131*, 9026−9037. (f) Benda, C. B.; Wang, J. Q.; Wahl, B.; Fässler, T. F. Syntheses and ^{1}H NMR spectra of substituted Zintl ions $[Ge_9R_n]^{(4-n)-}$: Crystal Structures of $[Ge_9R]^{3-}$ (R = 2,4,6-$Me_3C_6H_2$, $CHCH_2$) and indication of tris-vinylated clusters, *Eur. J. Inorg. Chem*, **2011**, 4262−4269. (g) Li, F.; Sevov, S. C. Rational synthesis of $[Ge_9\{Si(SiMe_3)_3\}_3]^{-}$ from its parent Zintl ion Ge_9^{4-}, *Inorg. Chem*. **2012**, *51*, 2706−2708. (h) Bentlohner, M. M.; Fard, Z. H.; Klein, W.; Jantke, L. A.; Fässler, T. F. Linking Deltahedral Zintl Clusters with Conjugated Organic Building Blocks: Synthesis and Characterization

of the Zintl Triad [R-Ge_9-CH=CH-CH=CH-Ge_9-R]$^{4-}$, *Angew. Chem. Int. Ed*. **2015**, *54*, 3748−3753; (i) Mayer, K..; Schiegerl, L. J.; Kratky, T ; Gunther, S.; Fässler, T. F, Targeted attachment of functional groups at Ge9 clusters via silylation reactions, *Chem. Commun*., **2017**, *53*, 11798-11801.

(26) (a) Schnepf, A. Metalloid cluster compounds of germanium: A novel class of germanium cluster compounds of formulae Ge_nR_m (n > m), *Coord. Chem. Rev*., **2006**, 250, 2758–2770. (b) Kysliak, O.; Schrenk, C.; Schnepf, A, The Largest Metalloid Group 14 Cluster, $Ge_{18}[Si(SiMe_3)_3]_6$: An Intermediate on the Way to Elemental Germanium, *Angew. Chem. Int. Ed*. **2016**, *55*, 3216 –3219. (c) Schenk, C.; Kracke, A.; Fink, K.; Kubas, A.; Klopper, W.; Neumaier, M.; Schnockel, H.; Schnepf, A.; The Formal Combination of Three Singlet Biradicaloid Entities to a Singlet Hexaradicaloid Metalloid $Ge_{14}[Si(SiMe_3)_3]_5[Li(THF)_2]_3$ Cluster, *J. Am. Chem. Soc*. **2011**, *133*, 2518–2524.

(27) (a) Schenk, C.; Schnepf, A, $[AuGe_{18}\{Si(SiMe_3)_3\}_6]^-$: A Soluble Au–Ge Cluster on the Way to a Molecular Cable?**, *Angew. Chem. Int. Ed*. **2007**, *46*, 5314 –5316. (b) Kysliak, O.; Schrenk, C.; Schnepf, A, Reactivity of $[Ge_9\{Si(SiMe_3)_3\}_3]^-$ Towards Transition-Metal M^{2+} Cations: Coordination and Redox Chemistry, *Chem. Eur. J*. **2016**, 22, 1–8. (c) Schenk, C.; Schnepf, A. $\{Ge_9R_3Cr(CO)_5\}^-$ and $\{Ge_9R_3Cr(CO)_3\}^-$: a metalloid cluster ($Ge_9R_3^-$) as a flexible ligand in coordination chemistry [R = $Si(SiMe_3)_3]^-$, *Chem. Commun*., **2009**, 3208–3210. (d) Henke, F.; Schenk, C.; Schnepf, A., $[Si(SiMe_3)_3]_6Ge_{18}M$ (M= Zn, Cd, Hg): neutral metalloid cluster compounds of germanium as highly soluble building blocks for supramolecular chemistry. *Dalton Trans*., **2009**, 9141–9145; (e) Mayer, K.; Jantke, L. A.; Schulz, S.; Fässler, T. F, Retention of the Zn-Zn bond in $[Ge_9Zn\text{-}ZnGe_9]^{6-}$ and Formation of $[(Ge_9Zn)\text{-}(Ge_9)\text{-}(ZnGe_9)]^{8-}$ and Polymeric $[\text{-}(Ge_9Zn)^{2-}\text{-}]^1$, *Angew. Chem. Int. Ed,* **2017**, 56, 2350–2355.

(28) (a) Li, F.; Munoz-Castro, A.; Sevov, S. C.; $[Ge_9\{Si(SiMe_3)_3\}_3\{SnPh_3\}]$: a tetrasubstituted and neutral deltahedral nine-atom cluster, *Angew. Chem.* **2012**, *51*, 8581–8584; (b) Li, F.; Sevov. S. C. Synthesis, structures, and solution dynamics of tetrasubstituted nine-atom germanium deltahedral clusters, *J. Am. Chem. Soc*, **2014**, *136*, 12056−12063 (c) Li, F.; Munoz-Castro, A.; Sevov, S. C. $[(Me_3Si)\ Si]_3EtGe_9Pd\ (PPh_3)$, a Pentafunctionalized Deltahedral Zintl Cluster: Synthesis, Structure, and Solution Dynamics, *Angew. Chem. Int. Ed*. **2016**, *55*, 8630–8633;

(29) (a) Perla, L. G.; Sevov, S. C. A stannyl-decorated Zintl ion $[Ge_{18}Pd_3(Sn^iPr_3)_6]^{2-}$: twinned icosahedron with a common Pd_3-face or 18-vertex *hypho*-deltahedron with a Pd_3-triangle inside, *J. Am. Chem. Soc*. **2016**, *138*, 9795−9798; (b) Perla, L. G.; Muñoz-Castro, A.; S Sevov, S. C, Eclipsed- and Staggered-$[Ge_{18}Pd_3\{E^iPr_3\}_6]^{2-}$ (E = Si, Sn): Positional Isomerism in Deltahedral Zintl Clusters, *J. Am. Chem. Soc*., 2017, 139, 15176–15181.

(30) Kesanli, B.; Fettinger, J.; Gardner, D. R.; Eichhorn, B. The $[Sn_9Pt_2(PPh_3)]^{2-}$ and $[Sn_9Ni_2(CO)]^{3-}$ complexes: two markedly different Sn_9M_2L transition metal Zintl ion clusters and their dynamic behavior, *J. Am. Chem. Soc*. **2002**, *124*, 4779–4786.

(31) Kocak, F. S.; Zavalij, P.; Eichhorn, B. Reactions of *exo*-substituted RSn_9^{3-} clusters with Pd: endohedral cluster formation and oxidative insertion, *Chem. Eur. J*. **2011**, *17*, 4858–4863.

(32) (a) Hlukhyy, V.; Stegmaier, Saskia.; Wüllen, L.; Fässler, T. F. Endohedrally Filled $[Ni@Sn_9]^{4-}$ and $[Co@Sn_9]^{5-}$ Clusters in the Neat Solids $Na_{12}Ni_{1-x}Sn_{17}$ and $K_{13-x}Co_{1-x}Sn_{17}$: Crystal Structure and 119Sn Solid-State NMR Spectroscopy. *Chem. Eur. J*. 2014, 20, 12157–12164. (b) He, H.; Klein, W.; Jantke, L. A.; Fässler, T. F. Metal-Centered Zintl Ions Isolated by Direct Extraction from Endohedral Intermetallic Precursor: $[Co_{1-x}@Sn_9]^{4-}$ (x ≈ 0.32) and $[Co_2@Sn_{17}]^{5-}$, *Z. Anorg. Allg. Chem.* 2014, 640, 2864–2870.

(33) Hong, X.; Cheung, K-K.; Guo C-X.; Che, C-M. Luminescent organometallic gold(I) complexes. Structure and photophysical properties of alkyl-, aryl- and μ-ethynylene gold(I) complexes, *J. Chem. Soc. Dalton. Trans*. **1994,** 1867-1871.

(34) (a) Sheldrick, G. M. SHELXT–Integrated Space-Group and Crystal-Structure Determination. *Acta Cryst*. **2015**, *A71*, 3-8. (b) Dolomnov O. V.; Bourhis L. J.; Gildea R. J.; Howard J. A. K.; Puschmann H.; OLEX2: A Complete Structure Solution, Refinement and Analysis Program. *J. Appl Cryst.* **2009**, *42*, 229–341; (c) Spek, A. L, Structure validation in chemical crystallography, *Acta Cryst.* **2009**, 148–155.

(35) (a) Te Velde, G.; Bickelhaupt, F. M.; Baerends, E. J.; Fonseca-Guerra, C.; Van Gisbergen, S. J. A.; Snijders, J. G.; Ziegler, T., Chemistry with ADF, *J. Comput. Chem.*, **2001**, *22*, 931–967. (b) Fonseca Guerra, C.; Snijders, J. G.; Te Velde, G.; Baerends, E. J., Towards an order-N DFT method, *Theor. Chem. Acc.*, **1998**, *99*, 391–403. (c) ADF2016, SCM, Theoretical Chemisty, Vrije Universiteit, Amsterdam, The Netherlans, http://www.scm.com.

(36) Perdew, J. P.; Burke, K.; Ernzerhof, M., Generalized Gradient Approximation Made Simple, *Phys. Rev. Lett.*, **1996**, *77*, 3865-3868.

(37) van Lenthe, E.; Baerends, E.J., Optimized Slater-type basis sets for the elements 1-118, *J. Comp. Chem.*, 2003, *24*, 1142-1156.

(38) (a) van Lenthe, E.; Baerends, E.J.;Snijders, J.G., Relativistic regular two-component Hamiltonians, *J. Chem. Phys.*, 1993, *99*, 4597-4610. (b) van Lenthe, E.; Baerends;Snijders, J.G., Relativistic total energy using regular approximations, *J. Chem. Phys.,*1994, *101*, 9783-9792. (c) van Lenthe, E.; Ehlers A.E.; Baerends, E.J., Geometry optimization in the Zero Order Regular Approximation for relativistic effects, *J. Chem. Phys*, 1999, *110*, 8943-8953.

(39) Pye, C.C.; Ziegler, T., An implementation of the conductor-like screening model of solvation within the Amsterdam Density Functional package, *Theor. Chem. Acc*., 1999, *101*, 396-408.

(40) (a) Fan, L.; Ziegler, T., Application of density functional theory to infrared absorption intensity calculations on main group molecules, *J. Chem. Phys.*, **1992**, *96*, 9005-9012. (b) Fan, L.;Ziegler, T., Application of density functional theory to infrared absorption intensity calculations on transition-metal carbonyls, *J. Phys. Chem.*, **1992**, *96*, 6937-6941.

(41) Bader, R. F. W. Atoms in molecules: a quantum theory. USA: Oxford University Press, **1994**.

(42) Bader, R. F. W. A quantum theory of molecular structure and its applications, *Chem. Rev*. **1991**, *91*, 893–928.

(43) Byers, L. R.; Ucbtman, V. A.; Dahl. L. F. Synthesis and stereochemical analysis of the triangular Cobalt-Dinickel clusters (η^5-$C_5H_{5-n}Me_n$)$CoNi_2(\eta^5$-$C_5H_5)_2(\mu_3$-$CO)_2$ (where n = 0, 1, 5): direct evidence for the antibonding trimetal character of the unpaired electron in the Fischer-Palm, *J. Am. Chem. Soc*. **1981**, *103*, 1942–1951.

(44) Ciabatti, L.; Femoni, C.; Iapalucci, M. C. Longoni, G.; Zacchini,

S. Bimetallic Nickel–Cobalt hexacarbido carbonyl clusters $[H_{6-n}Ni_{22}Co_6C_6(CO)_{36}]^{n-}$ (n = 3–6) possessing polyhydride nature and their base-induced degradation to the monoacetylide $[Ni_9CoC_2(CO)_{16-x}]^{3-}$ (x = 0, 1), *Organometallics*. **2012**, *31*, 4593−4600.

(45) Liu, C.; Li, L. J.; Pan, Q. J.; Sun, Z. M.; $[Ge_5Ni_2(CO)_3]^{2-}$：The first functionalized cluster of closo-$[Ge_5]^{2-}$, *Chem. Commun*., **2017**，53, 6315-6318.

(46) Emoni, C.; Lapalucci, M. C.; Longoni, G.; Wolowska, J.; Zacchini, S.; Zanello, P.; Fedi, S.; Ricco, M.; Pontiroli, D.; Mazzani, M. Magnetic behavior of odd- and even-electron metal carbonyl clusters: the case study of $[Co_8Pt_4C_2(CO)_{24}]^{n-}$ (n = 1, 2) carbide cluster, *J. Am. Chem. Soc*. **2010**, *132*, 2919–2927.

(47) Ciabatti, L.; Femoni, C.; Hayatifar, M.; Lapalucci, M. C.; Lenco, A.; Longoni, G.; Manca, G.; Zacchini, S. Octahedral Co-carbide carbonyl clusters decorated by $[AuPPh_3]^+$ fragments: synthesis, structural isomerism, and aurophilic interactions of $Co_6C(CO)_{12}(AuPPh_3)_4$, *Inorg. Chem*. **2014**, *53*, 9761−9770.

For Table of Contents Use Only

Reactivity Studies of $[Co@Sn_9]^{4-}$ towards Transition Metal Reagents: A Bottom-Up Synthesis of Ternary Functionalized Zintl Clusters

Chao Liu, Lei-Jiao Li, Xiao Jin, John E. McGrady, and Zhong-Ming Sun

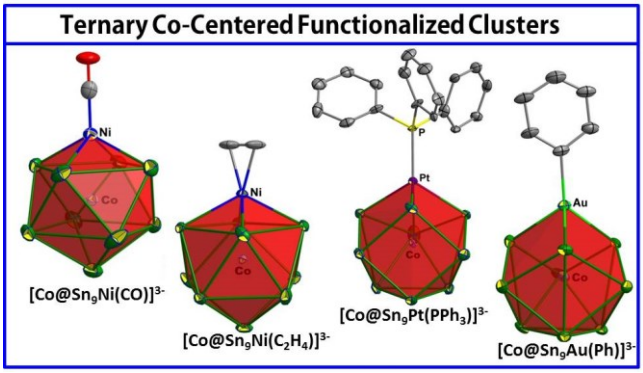

A family of Co-centered metal fragments functionalized cluster anions, $[Co@Sn_9Ni(CO)]^{3-}$, $[Co@Sn_9Ni(C_2H_4)]^{3-}$, $[Co@Sn_9Pt(PPh_3)]^{3-}$ and $[Co@Sn_9AuPh]^{3-}$, have been synthesized using the K-Co-Sn phase as the precursor.